Ocean Dynamics
DOI 10.1007/s10236-005-0043-0

Henk A. Dijkstra · Lianke te Raa · Maurice Schmeits · Jeroen Gerrits

On the physics of the Atlantic Multidecadal Oscillation

Received: 29 July 2005 / Accepted: 9 November 2005

Abstract The Atlantic Multidecadal Oscillation (AMO) is a pronounced signal of climate variability in the North Atlantic sea-surface temperature field. In this paper, we propose an explanation of the physical processes responsible for the timescale and the spatial pattern of the AMO. Our approach involves the analysis of solutions of a hierarchy of models. In the lowest member of the model hierarchy, which is an ocean-only model for flow in an idealized basin, the variability shows up as a multidecadal oscillatory mode which is able to destabilize the mean thermohaline circulation. In the highest member of the model hierarchy, which is the Geophysical Fluid Dynamics Laboratory R30 climate model, multidecadal variability is found as a dominant statistical mode of variability. The connection between both results is established by tracing the spatial and temporal expression of the multidecadal mode through the model hierarchy while monitoring changes in specific quantities (mechanistic indicators) associated with its physics. The proposed explanation of the properties of the AMO is eventually based on the changes in the spatial patterns of variability through the model hierarchy.

Responsible Editor: Tal Ezer

H. A. Dijkstra (✉) · L. te Raa
Institute for Marine and Atmospheric Research Utrecht,
Utrecht University,
3766 HW Utrecht,
The Netherlands
e-mail: dijkstra@phys.uu.nl

M. Schmeits
Royal Netherlands Meteorological Institute,
De Bilt,
The Netherlands

J. Gerrits
College of Oceanic and Atmospheric Sciences,
Oregon State University,
Corvallis, OR, USA

Introduction

The North Atlantic sea-surface temperature (SST) appears to have a distinct signal of multidecadal variability (Bjerknes 1964; Folland et al. 1984; Schlesinger and Ramankutty 1994). The difference of the SST pattern between the relatively warm years 1950–1964 and the relatively cold years 1970–1984 shows negative anomalies near Newfoundland and positive anomalies over the rest of the basin (Kushnir 1994). By subsequent analysis of longer and better quality SST and sea-level pressure (SLP) data, the pattern of multidecadal variability has been characterized more accurately (Moron et al. 1998; Tourre et al. 1999). Delworth and Mann (2000) extended the instrumental record with proxy data and demonstrated that there is a significant spectral peak in the 50- to 70-year frequency band. The variability was named the Atlantic Multidecadal Oscillation (AMO) in Kerr (2000), and an AMO index was defined in Enfield et al. (2001) as the 10-year running mean of the detrended Atlantic SST anomalies north of the equator.

Although detailed mechanisms are not clear in most cases, there appear to be climate variations which are well correlated with the AMO. Enfield et al. (2001) showed that there is a significant negative correlation with US continental rainfall, with less (more) rain over most of the central USA during a positive (negative) AMO index period. For example, the Mississippi outflow is about 5% less than average during a positive AMO phase. High positive correlations have been found between the AMO and Sahel rainfall and between the AMO and hurricane intensity in the Atlantic (Gray et al. 1997). During the positive AMO index period 1950–1964, there were 47 intense (class 3, 4, 5) hurricanes originating east of 60°W. In the same length (negative AMO index) period 1970–1984, there were only 19. Multidecadal variability has also been identified in long-term observations of sea-ice concentration in the Arctic (Venegas and Mysak 2000). The periods where the sea-ice concentration is lower (higher) than average roughly coincide with periods of positive (negative) AMO index. Recently, Sutton and Hodson (2005) investigated the northern hemispheric

climate impacts of the AMO and demonstrated that the difference in summer precipitation pattern between positive and negative AMO states shows a 5–15% increase over Western Europe. The difference pattern in atmospheric surface temperatures shows warm anomalies over the USA and over central Europe.

North Atlantic multidecadal climate variability has also been found in coupled ocean–atmosphere models. Delworth et al. (1993) analyzed a 600-year simulation of the Geophysical Fluid Dynamics Laboratory (GFDL) R15 climate model. They found an average period of about 50 years in the strength of the thermohaline circulation (THC) as measured by a THC index, i.e., the maximum of the Atlantic's meridional overturning streamfunction. The SST difference between high- and low-THC-index states is in reasonable agreement with the pattern derived from observations (Kushnir 1994). Further analysis of the GFDL-R15 results (Delworth et al. 1993) showed that the multidecadal variability is associated with a coupling between the density anomalies in the sinking region (of the THC) and the strength of the Atlantic meridional overturning circulation.

The GFDL-R15 model is not the only coupled general circulation model (GCM) in which Atlantic multidecadal variability has been found. In the Max Planck Institute Ocean Model 1 (MPI-OM1) (Latif et al. 2004), irregular variability is found with a mean period of about 50 years and an amplitude in SST about twice as large as in observations. The spatial pattern of SST anomalies (Fig. 2b in Latif et al. 2004) is similar to that in observations and in the GFDL-R15 model. Dong and Sutton (2005) found multidecadal variability in the HadCM3 model with an average period of about 24 years. Analysis of the lag correlation between different fields (SST, mixed layer depth, salinity anomalies, etc.) leads to the description of a similar mechanism as that in Delworth et al. (1993), although the timescale of variability is about half as that in the GFDL-R15 model.

A nice set of sensitivity simulations with the GFDL-R15 model was presented by Delworth and Greatbatch (2000). They showed that when the ocean model is forced by the climatological seasonal cycle of surface fluxes, no multidecadal variability is found. When the ocean model is forced by annual-mean surface fluxes (allowing atmospheric "noise" in the surface fluxes), the variability is similar to that of the coupled model. The heat flux is shown to be the essential component of the surface fluxes causing the variability. It is concluded that the multidecadal variability can be attributed to "a damped mode in the ocean system, which is continuously excited by low-frequency atmospheric forcing." Although this is an important result, it provides neither a mechanistic description for the physical processes setting the timescale of the AMO nor an explanation for its spatial pattern.

The results in Delworth et al. (1993) and Delworth and Greatbatch (2000) suggest that the essential physics of the multidecadal variability can be understood from ocean-only models. Indeed, multidecadal oscillations have been found in many idealized sector models of the three-dimensional ocean circulation, forced by only a surface heat flux (Greatbatch and Zhang 1995; Greatbatch and Petersen 1996; Chen and Ghil 1996). From these studies, it appears that a phase difference between changes in the meridional overturning circulation and the resulting temperature anomalies is essential to the variability. Moreover, critical thresholds also exist: for example, when the horizontal mixing of heat is too large, no multidecadal oscillations are found.

By studying the sensitivity of the multidecadal oscillations to the representation of convective adjustment, the thermal and momentum boundary conditions, the coupling to the atmosphere, and the representation of mesoscale variability, Huck and coworkers (Colin de Verdière and Huck 1999; Huck et al. 1999) showed that the multidecadal oscillations exist under a wide range of conditions. Both Huck and Vallis (2001) and Te Raa and Dijkstra (2002) concluded that the threshold behavior is associated with a Hopf bifurcation, in which a multidecadal mode destabilizes the thermally driven steady flow. The physical mechanism of growth and propagation of this mode was described from the patterns near the Hopf bifurcation (Te Raa and Dijkstra 2002). The multidecadal mode also exists in a coupled ocean–atmosphere model, but it is damped over the volume in parameter space investigated (Te Raa and Dijkstra 2003b).

Te Raa et al. (2004) studied finite amplitude transient flows displaying multidecadal variability in the single-hemispheric basin configuration with and without "realistic" continental boundaries. They showed that in situations with continental geometry, the variability still originates from the same physical processes as in the idealized model, although the patterns of variability become strongly deformed. The work in Te Raa and Dijkstra (2002) provides strong motivation for trying to connect the variability in the ocean-only models to that found in coupled GCMs such as the GFDL climate model (Delworth et al. 1993; Delworth and Greatbatch 2000). In this paper, we attempt to establish such a connection and propose an explanation for the timescale and spatial pattern of multidecadal variability in these models and in observations.

The main idea pursued here is to trace the spatial and temporal characteristics of the multidecadal mode in Te Raa and Dijkstra (2002) through a model hierarchy while monitoring so-called mechanistic indicators to see if changes in the physics of the variability occur. First, we first analyze the multidecadal variability in the results of a 900-year simulation with the GFDL-R30 climate model. Next, we start with the results in Te Raa and Dijkstra (2002) and shortly recall the physical mechanism of the multidecadal mode as a necessary step to introduce the mechanistic indicators. Subsequently, the indicators are used to explain the physics of multidecadal variability in finite amplitude ocean flows. The connection between these results leads to the proposed explanation of the AMO which is discussed in the last section.

Statistical modes in the GFDL-R30 model

The GFDL-R30 model consists of general circulation models of both the atmosphere and ocean, with relatively simple formulations of land-surface and sea-ice processes (Delworth et al. 2002). The atmospheric portion of the coupled model solves the primitive equations on the sphere using a spectral technique with rhomboidal 30 truncation, which corresponds to a resolution of approximately 3.75° longitude by 2.25° latitude. There are 14 unevenly spaced levels in the vertical. The ocean component of the coupled model uses version 1.1 of the Modular Ocean Model (MOM). The resolution of this component is 1.875° longitude by 2.25° latitude, with 18 unevenly spaced levels in the vertical. The governing equations are solved numerically with the use of the Boussinesq, rigid-lid, and hydrostatic approximations; flux correction is applied to limit drift in the model.

The model output used in this study [generously provided to us by Tom Delworth (GFDL, Princeton)] is from the most stable control run of the GFDL-R30 model as described in Delworth et al. (2002). Although the model was integrated for 900 years, we have only analyzed the last 500 years (years 401–900) because of substantial drift in the first 400 years of the simulation. Fields analyzed were the annual-mean potential temperature, potential density, salinity, and horizontal velocity at five vertical levels [level 1 (20 m), level 6 (301 m), level 9 (683 m), level 12 (1,456 m), and level 15 (2,798 m)] and the meridional overturning in the Atlantic. The meridional overturning streamfunction (Ψ) is computed from:

$$\Psi(\theta,z,t) = \int_{z_b}^{z} \int_{99^\circ W}^{2^\circ W} v(\phi,\theta,z',t) \cos\theta \, d\phi dz', \qquad (1)$$

where z_b is the bottom depth and v is the meridional velocity. The model shows fairly realistic climatological annual-mean (averaged over model years 401–900) SST and salinity fields with the temperature effect dominating (i.e., giving the largest contribution to) the potential density (Delworth et al. 2002). The simulated maximum meridional overturning of 25 sverdrup (Sv) is quite high, compared to that deduced from observations, and the sinking mainly occurs between 60° and 65°N.

Multichannel Singular Spectrum Analysis (M-SSA) (Plaut and Vautard 1994) was performed on the annual-mean potential temperature, salinity, horizontal velocities, and potential density fields at the five vertical levels mentioned above and on the meridional overturning streamfunction in the North Atlantic region. The analysis has been performed for each field separately, and in all cases described below, the annual-mean anomalies were prefiltered with standard principal component analysis (PCA; Preisendorfer 1988) in order to reduce the number of spatial degrees of freedom. The leading ten principal components (PCs), which account for 63–99% of the variance, provide the L input channels for the M-SSA analysis. We have used 500 years of data (N=500) and a standard window length M of 100 years.

In the meridional overturning, the dominant timescale of variability is 44 years, and this result is statistically significant at the 95% confidence level. The 44-year timescale belongs to space–time principal component (ST-PC) pair 1–2 that is in quadrature, which indicates that the pair represents the dominant oscillatory statistical mode. This ST-PC pair explains 42% of the variance in the ten leading PCs of the meridional overturning. We have checked the robustness of this 44-year statistical mode with respect to different values of the window length (M=50 and M=75).

The maximum values of Ψ (Ψ_M) of the reconstructed component (RC) 1–2 are plotted in Fig. 1a. The anomaly patterns corresponding to RC 1–2 of the meridional overturning are shown in Fig. 1b–e for four phases during the oscillation. The starting time was chosen to be year 600, when the amplitude of Ψ_M of the statistical mode is near maximal, and each subsequent picture is 6 years later. Together, the pictures show nearly half of the cycle of the oscillation, and the other half-cycle is similar but with anomalies of reversed sign. In Fig. 1b, the overturning anomaly Ψ_M is about 2.5 Sv stronger than its average value, with a single-cell anomaly pattern. After 6 years, the overturning anomaly has slightly decreased (Fig. 1c) while keeping the same pattern. The anomaly is nearly zero after about 12 years (Fig. 1d), and after 18 years, the overturning is weaker than normal (Fig. 1e), again with the same anomaly pattern.

In all the annual-mean fields (at all levels) analyzed with M-SSA, the dominant oscillatory mode has a timescale of 44 years. Some of the model fields at deeper levels show a trend as the first M-SSA ST-PC. This indicates that the deeper part of the model ocean is still not fully in equilibrium. All subsequent figures representing the reconstructed anomaly patterns of the analyzed quantities of the statistical multidecadal mode have the same starting time (i.e., year 600) and the same time increment (i.e., 6 years) between the panels as chosen for Fig. 1.

By analyzing the RC 1–2 anomaly patterns of the potential temperature and salinity at level 1, it appears that the near-surface potential density anomalies are almost everywhere dominated by near-surface salinity anomalies. In addition, it is found that temperature and salinity anomalies are (pointwise) approximately in phase. As an example, we plot the temperature and salinity anomalies at the two locations, 40°W, 56°N (Fig. 2a) and 56°W, 40°N (Fig. 2b). A positive salinity anomaly is accompanied by a positive temperature anomaly, so both are partially compensating in the density anomaly. In the RC 1–2 anomaly patterns of the potential temperature, a positive anomaly is slightly propagating in a southwestward direction from the southern tip of Greenland to the south of Newfoundland, where it is dissipated. Because the pattern of the salinity anomalies is similar to that of the temperature anomalies, we consider only potential density anomalies below.

Figure 3 presents the RC 1–2 anomaly patterns of the potential density and the horizontal velocity at level 1

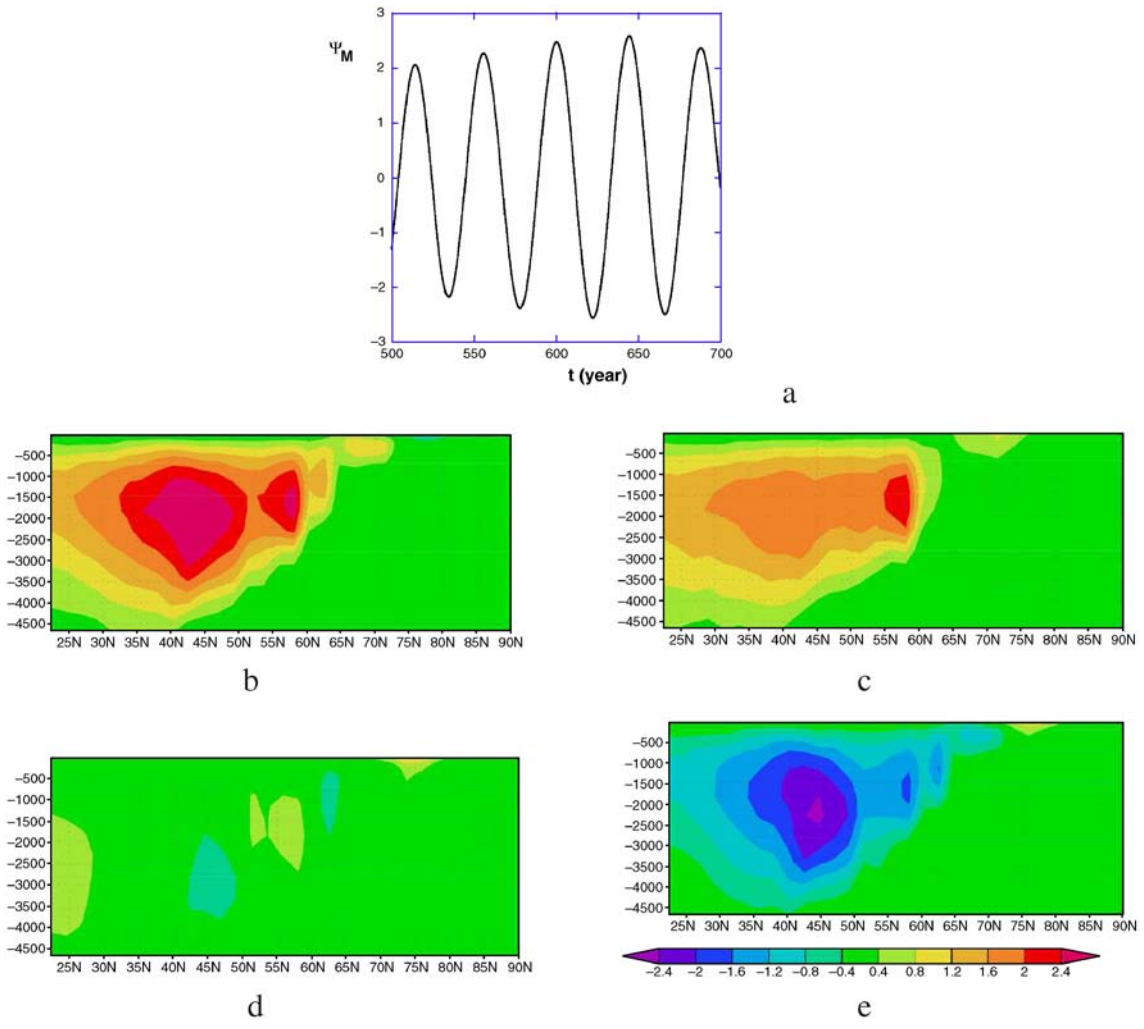

Fig. 1 Reconstructed component (RC) pair 1–2 of the meridional overturning streamfunction in the North Atlantic region describing the oscillatory statistical mode having a 44-year timescale. **a** Amplitude of maximum meridional streamfunction anomaly (sverdrup) of the mode. **b**–**e** Spatial patterns of the meridional streamfunction anomaly shown at 6-year intervals, starting in model year 600, over about one half-cycle of the oscillation; the other half-cycle is similar but with anomalies of reversed sign. **b** year 600, **c** year 606, **d** year 612, and **e** year 618

(20-m depth) for four phases during the oscillation. Figure 3a corresponds to the phase where the meridional overturning anomaly has a maximum. In this phase, the potential density to the south and west of Greenland also has a maximum and decreases thereafter (Fig. 3b–d). In the phase where the meridional overturning anomaly has a maximum (cf. Fig. 1b), the simulated Gulf Stream is anomalously strong and the East Greenland Current anomalously weak (Fig. 3a), consistent with positive near-surface salinity, density, and convection anomalies (Delworth and Mann 2000). At year 612 (Fig. 3c), there is a clear signature of an anomalous anticyclonic circulation east of Newfoundland that is induced by the positive temperature anomalies.

Figure 4 represents the RC 1–2 anomaly patterns of the potential density and the horizontal velocity field at level 9 (683-m depth) for four phases during the oscillation. What is most striking in this figure is that the spatial patterns of the potential density at this level are quite different from those at a depth of 20 m. In fact, the density anomalies are now dominated by potential temperature anomalies instead of salinity anomalies (which are now very small), and they propagate in a (south) westward direction. The horizontal velocity patterns in Fig. 4 are quite similar to those at level 1 and are caused by the density anomalies. At year 612, there is again the signature of the anomalous anticyclonic circulation east of Newfoundland, induced by the positive temperature anomaly (i.e., the negative density anomaly in Fig. 4c). This anomalous circulation is present in the upper 1,000 m of the central North Atlantic. The intensity of this circulation lags the intensity of the meridional overturning by approximately 10 years, similar to that found in Delworth and Mann (2000).

The RC 1–2 anomaly patterns of the potential density at levels 6 (301 m), 12 (1,456 m), and 15 (2,798 m) also show a westward phase propagation. However, while the potential density anomalies at level 6 are dominated by potential temperature anomalies, the ones at levels 12 and 15 are

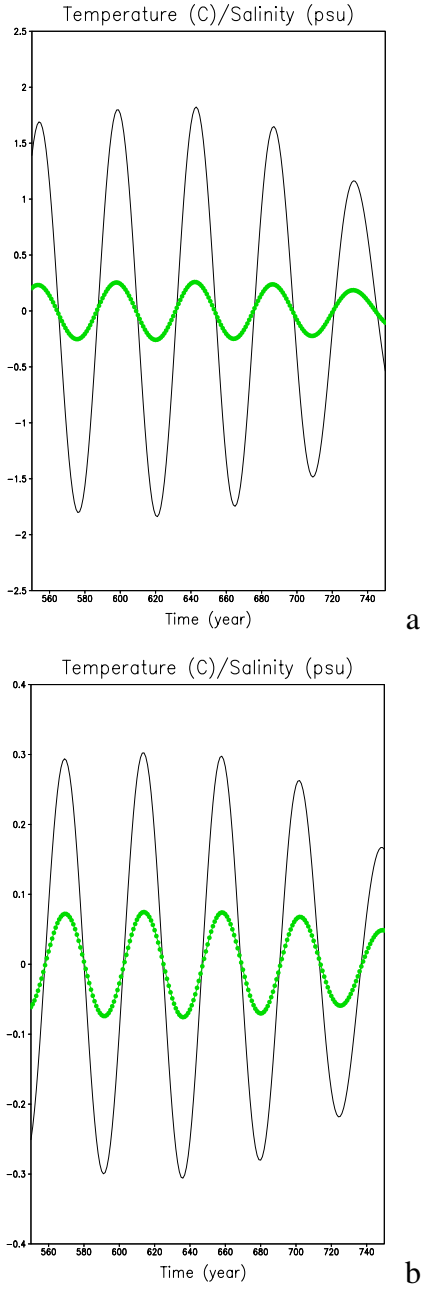

Fig. 2 Surface temperature (*black*) and surface salinity anomaly (*green*) associated with the RC pair 1–2 at the locations **a** 40°W, 56°N and **b** 56°W, 40°N

dominated by salinity anomalies. The propagation characteristics of temperature and salinity anomalies of the RC pair 1–2 are substantially different at the surface than at depth. Near the surface, where the signal has the largest amplitude, there is only a slight westward propagation of density anomalies, giving the impression of a near-standing spatial pattern of oscillation. At middepth, however, there is substantial westward propagation of potential density anomalies.

From observations, the only characteristics which are available of the AMO are its timescale (~50 years) and its spatial pattern (Fig. 5a) as obtained by Kushnir (1994). To establish a connection between these results and the GFDL model results, we determined the SST anomaly fields between Atlantic warm (corresponding to maximum meridional overturning) and Atlantic cold (corresponding to minimum meridional overturning) states for the dominant M-SSA mode in the GFDL-R30 model (Fig. 5b). There is a qualitative correspondence between the patterns in Fig. 5a and b with respect to: (1) the secondary maximum in the warm anomaly near 70°W, 30°N; (2) the area of negative anomalies near the North American coast; and (3) the pattern of the positive anomalies. There are also discrepancies, in particular, in the eastern basin, where the pattern of the observations shows positive anomalies and the GFDL-R30 pattern has slightly negative anomalies. In addition, the amplitude of the GFDL-R30 pattern is a factor 2–5 times larger than that in the observations.

To characterize the phase differences associated with the propagation of the pattern, we plot in Fig. 6 the temperature anomalies at two locations (40°W, 56°N and 56°W, 40°N) for both the surface level (Fig. 6a) and at 683-m depth (Fig. 6b). Near the surface, the phase difference between the anomalies is about 15 years or one third of the period; at 683 m, this phase difference has increased to about 20 years. The difference in the amplitude of the temperature anomalies is small at depth, while at the surface, the temperature anomalies are substantially greater at the northerly location. Having characterized the results of the GFDL model and encouraged by the good comparison with respect to observations, we now try to understand the physical processes causing the timescale, pattern, and propagation of the anomalies.

Idealized ocean-only models

First, we briefly recapitulate the basic physical mechanism of the multidecadal variability as found from studies in ocean-only models. From this description, quantities which characterize the physics of the variability, so-called mechanistic indicators, are introduced. Next, we discuss the issue of sustained vs noise-driven oscillations to motivate our use of prescribed flux conditions for the temperature in subsequent sections.

Basic physics and mechanistic indicators

In many ocean-only models, it is found that a steady state determined under restoring temperature forcing displays multidecadal oscillations under prescribed flux conditions. Chen and Ghil (1995) already provided indications that this oscillatory flow arises through a Hopf bifurcation. The existence of the Hopf bifurcation was demonstrated by solving the linear stability problem of the three-dimensional flow (Huck and Vallis 2001; Te Raa and Dijkstra 2002). As control parameter, the horizontal mixing coefficient of heat, K_H, was used. The stability problem of both the steady state under restoring and prescribed flux

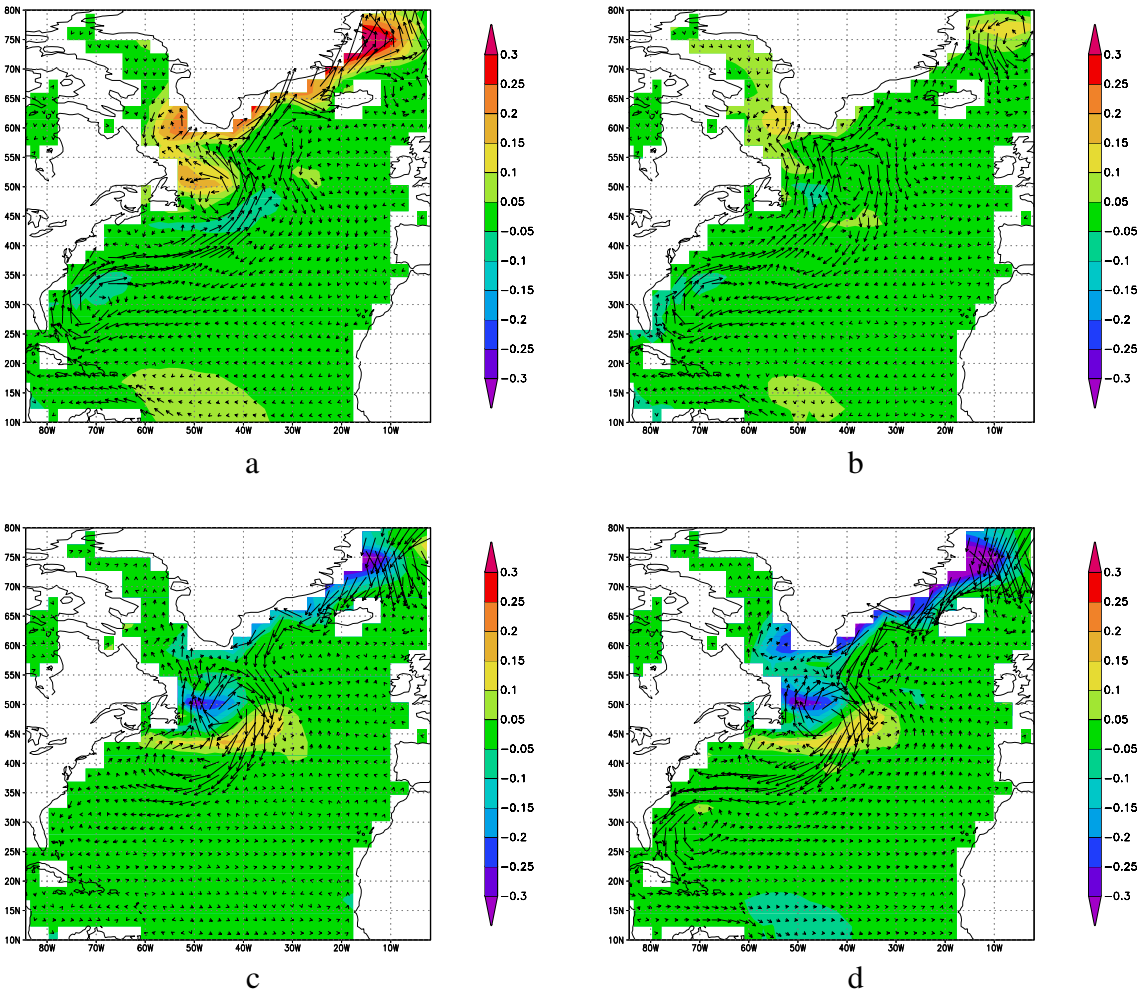

Fig. 3 RC pair 1–2 of potential density (kilogram per cubic meter) and horizontal velocity (centimeter per second) at level 1 in the North Atlantic region describing the oscillatory statistical mode having a 44-year timescale. The patterns are shown at 6-year intervals, starting in model year 600, over about one half-cycle of the oscillation; the other half-cycle is similar but with anomalies of reversed sign. **a** year 600, **b** year 606, **c** year 612, and **d** year 618

conditions was solved vs K_H; for both cases, the multidecadal mode exists. Largest growth factors are obtained in the case of prescribed heat flux conditions, where the atmospheric damping of thermal anomalies is effectively zero (Te Raa and Dijkstra 2003a); a nonzero atmospheric damping decreases the growth factor. A larger value of K_H also decreases the growth factor. The period of the mode depends on the atmospheric forcing and on mixing coefficients of heat, according to results in Huck and Vallis (2001) and Te Raa and Dijkstra (2002).

The great advantage of the linear stability analysis as in Te Raa and Dijkstra (2002) is that the propagation and growth mechanism of the multidecadal mode can be described from the eigenfunctions near the Hopf bifurcation. To introduce the idea of a mechanistic indicator, first a slight generalization (compared to that in Te Raa and Dijkstra 2002) of the propagation mechanism of temperature anomalies of the multidecadal mode is given in Fig. 7. A warm anomaly in the north-central part of the basin causes a positive meridional perturbation temperature gradient, which induces—via the thermal wind balance—a negative zonal surface flow (Fig. 7a). The anomalous anticyclonic circulation around the warm anomaly causes southward (northward) advection of cold (warm) water to the east (west) of the anomaly, resulting in westward phase propagation of the warm anomaly. Due to this westward propagation, the zonal perturbation temperature gradient becomes negative, inducing a negative surface meridional flow (Fig. 7b). The resulting upwelling (downwelling) perturbations along the northern (southern) boundary cause a negative meridional perturbation temperature gradient, inducing a positive zonal surface flow, and the second half of the oscillation starts. The crucial elements in this oscillation mechanism are the phase difference between the zonal and meridional surface flow perturbations and the westward propagation of the temperature anomalies (Te Raa and Dijkstra 2002).

The mechanism provides characteristics of the variability which one may try to determine in more complex models. These characteristics should be simple enough to be able to compute them over a hierarchy of models, yet complex enough to preserve the essential information

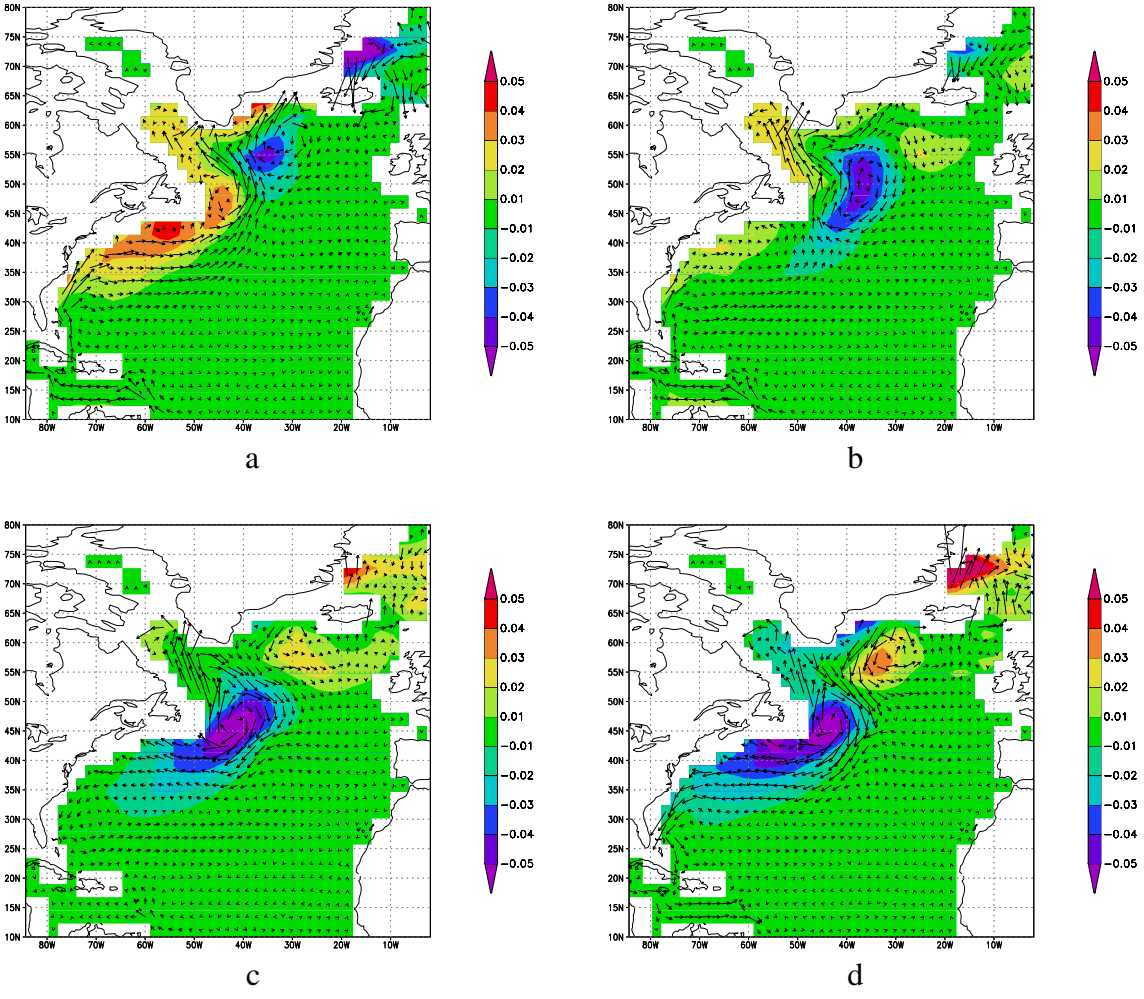

Fig. 4 RC pair 1–2 of potential density (kilogram per cubic meter) and horizontal velocity (centimeter per second) at level 9 in the North Atlantic region describing the oscillatory statistical mode having a 44-year timescale. The patterns are shown at 6-year intervals, starting in model year 600, over about one half-cycle of the oscillation; the other half-cycle is similar but with anomalies of reversed sign. **a** year 600, **b** year 606, **c** year 612, and **d** year 618

about the mechanism; we call them mechanistic indicators. Although the physical mechanism of the variability is probably best characterized by energy conversion principles (Te Raa and Dijkstra 2002), those quantities are difficult to compute over a hierarchy of models. Instead, two mechanistic indicators can be based directly on the propagation mechanism of the multidecadal mode as sketched in Fig. 7:

- M1: the phase difference between east–west and north–south temperature differences
- M2: the phase difference between zonal and meridional overturning anomalies

Both mechanistic indicators were already used in Te Raa et al. (2004). In the idealized case of thermally driven flow in a single-hemispheric ocean basin, M1 yields that the east–west temperature difference leads the north–south temperature difference by about a quarter of an oscillation period, whereas M2 yields that the meridional overturning anomaly lags the zonal overturning anomaly by a quarter to one third of an oscillation period.

Finite amplitude flows

The existence of the multidecadal mode and the Hopf bifurcation occurring under prescribed flux conditions has major implications for the time-dependent behavior of the flows. In this subsection, the different responses under subcritical (K_H values larger than that at the Hopf bifurcation) and supercritical (K_H values smaller than that at the Hopf bifurcation) conditions are studied.

This issue requires computation of transient, finite amplitude flows. Apart from the THCM model used in Te Raa and Dijkstra (2002), we also use version 3.1 of the GFDL MOM. In these computations, the same single-hemispheric 64°×64° basin as in Te Raa et al. (2004) is considered having a uniform depth D=4,000 m. A spatial

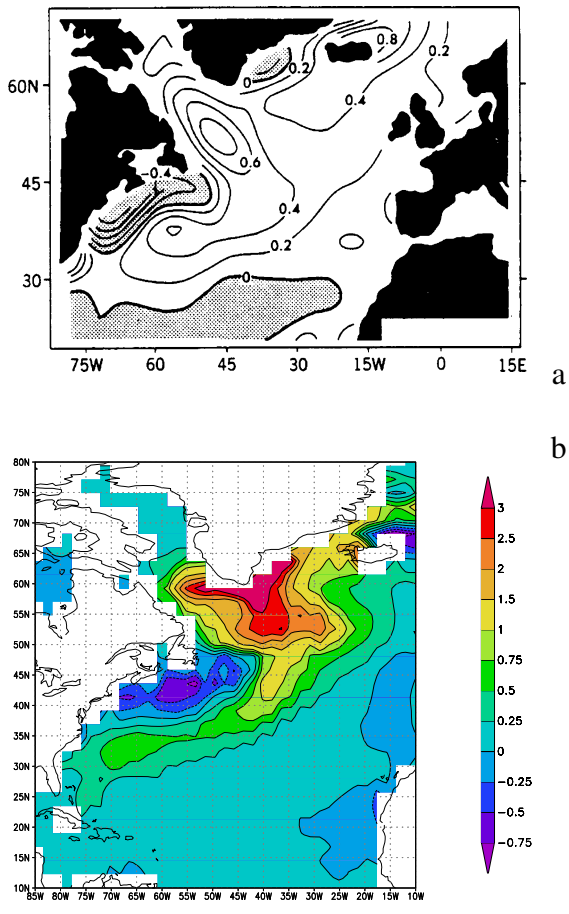

Fig. 5 **a** Observed pattern of the difference in North Atlantic sea-surface temperature (in degrees Celsius) between the relatively warm period 1950–1964 and the relatively cold period 1970–1984 (Kushnir 1994). **b** Difference in SSTs between the maximum and minimum meridional overturning for the statistical multidecadal mode in the GFDL-R30 model

horizontal resolution of 4°×4° with 16 equidistant vertical levels is used. The surface forcing is only thermal with an atmospheric temperature profile given by:

$$T_S(\theta) = T_0 + \frac{\Delta T}{2} \cos \pi \frac{\theta - \theta_s}{\theta_n - \theta_s}, \qquad (2)$$

where θ_s=10°N and θ_n=74°N are the southern and northern latitude of the domain, T_0=15°C is a reference temperature, and ΔT=20°C is the equator-to-pole temperature difference. The restoring timescale is 30 days, and the values of the vertical mixing coefficients of heat (K_V) and of momentum (A_V) are fixed at K_V=2.3×10^{-4} m^2 s^{-1} and A_V=1.0×10^{-3} m^2 s^{-1}; values of the other mixing coefficients are specified below.

Under prescribed flux conditions, we know from Fig. 7 in Te Raa et al. (2004) that the Hopf bifurcation is located near K_H^c=1,670 m^2 s^{-1} when the horizontal mixing coefficients of momentum A_H=1.6×10^7 m^2 s^{-1}. Consider now a steady flow computed under restoring conditions (using Eq. 2) with the MOM model for K_H=700 m^2 s^{-1}.

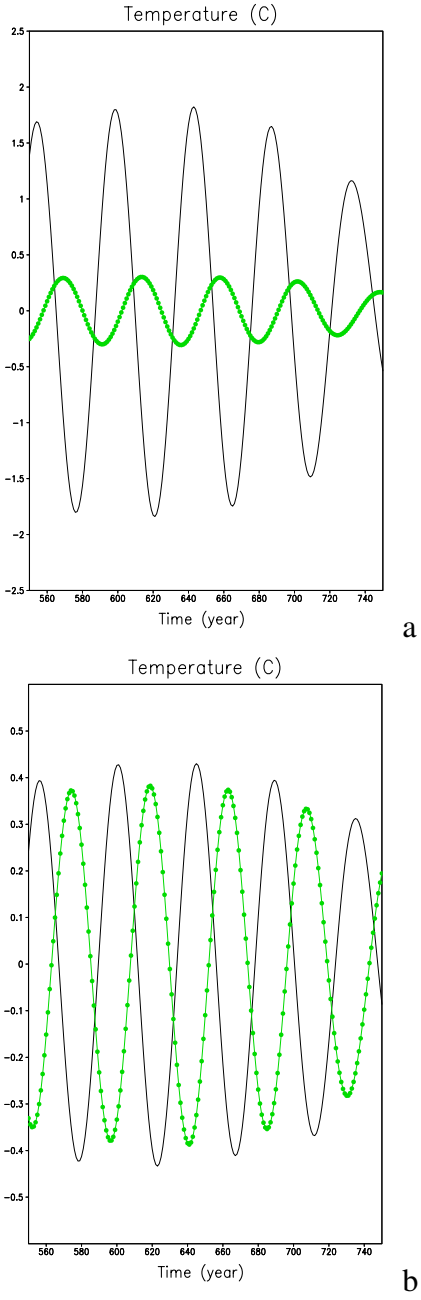

Fig. 6 Temperature anomalies at the locations 40°W, 56°N (*black*) and at 56°W, 40°N (*green*) associated with the multidecadal statistical mode in the GFDL-R30 model for **a** surface level and **b** 683-m depth

When after 3,000 years, the heat flux is diagnosed of this equilibrium solution and next prescribed as a flux boundary condition, sustained oscillations develop. The maximum meridional overturning streamfunction Ψ_M displays regular periodic variability with a period of about 50 years (Fig. 8a). This periodic orbit (also called a limit cycle) necessarily exists because of the presence of the super-critical Hopf bifurcation, as the value of K_H<K_H^c.

Now consider the subcritical case K_H=1,800 m^2 s^{-1} and a forcing which consists of the diagnosed steady heat flux plus a white noise component. The latter has a maximum

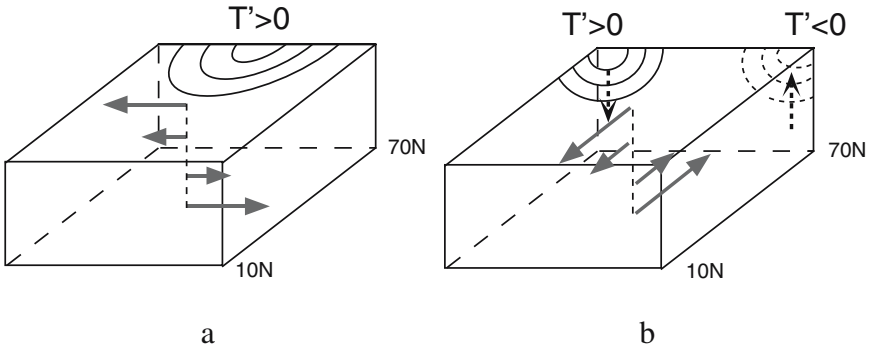

Fig. 7 Schematic diagram of the oscillation mechanism associated with the multidecadal mode. The phase difference between **a** and **b** is about $\pi 2$. See text and Te Raa and Dijkstra (2002) for further explanation

amplitude of 10% of the deterministic heat flux. This forced problem was integrated in time using the THCM model. The maximum meridional overturning streamfunction Ψ_M displays variability on many timescales, and a spectrum of this time series is plotted in Fig. 8b. Enhanced spectral energy appears in the multidecadal frequency band. In fact, the peak of the spectrum is centered around the period (about 70 years) of the damped multidecadal mode for K_H=1,800 m^2 s^{-1}. Hence, in this subcritical case ($K_H > K_H^c$), the multidecadal mode is damped, but its spatial and temporal characteristics can be excited by atmospheric noise. It is unfortunately not easy to establish the quantitative connection between the damping rate of a mode (in this case, the multidecadal mode) and the amplitude of the spectral peak in a noise-driven system (as here in Fig. 8b), given the amplitude of the noise forcing (Griffies and Tziperman 1995; Jin 1997).

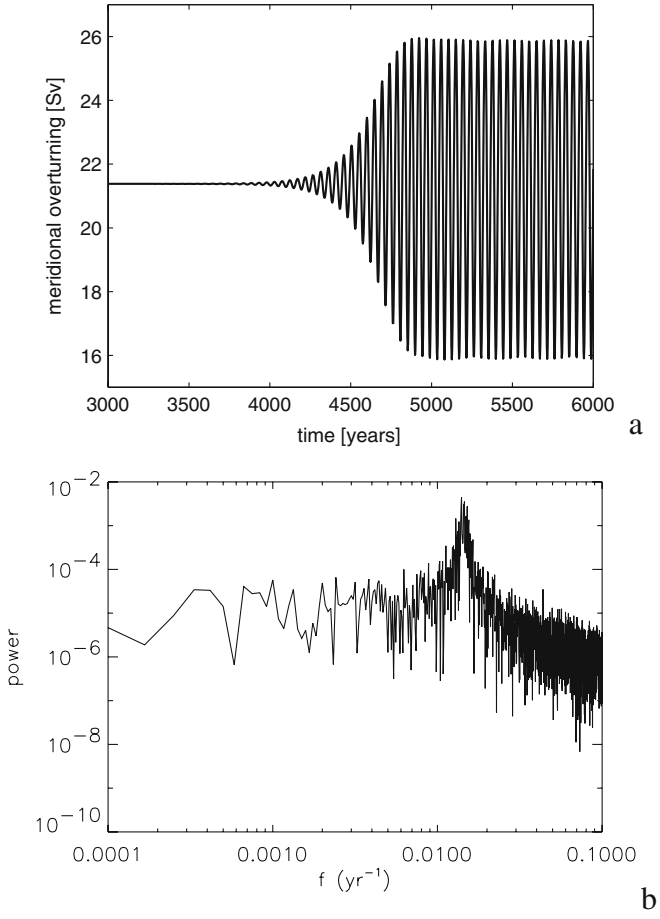

Fig. 8 **a** Periodic orbit, shown through the maximal meridional overturning, computed under prescribed flux conditions for K_H=700 m^2 s^{-1}. **b** Fourier spectrum of the meridional overturning anomaly in the case K_H=1,800 m^2 s^{-1} under white noise forcing. In these computations, the value of A_H=1.6×10^7 m^2 s^{-1}

As the multidecadal spatial and temporal variability is associated with one particular damped mode, one should be able to extract its spatial/temporal characteristics by statistical techniques which are specially designed to find propagating patterns in noisy data, such as the M-SSA algorithm (Plaut and Vautard 1994). Indeed, applying M-SSA to the fields from the noise-driven flow, one finds a significant statistical mode with the same period of the multidecadal mode and the same pattern as the eigenmode Te Raa and Dijkstra (2003a).

Actually, there is quite a strong qualitative connection between the results here and those for El Nino Southern Oscillation (ENSO) variability in intermediate complexity tropical ocean–atmosphere models (Neelin et al. 1998). In these models, there is also an underlying mode of variability (the ENSO mode) which can destabilize the Pacific mean state through a Hopf bifurcation once the coupling parameter is increased. Hence, there is a subcritical regime where the ENSO mode is damped and the mean equatorial climate state is stable, and there is a supercritical regime where there is a sustained oscillation. In Roulston and Neelin (2000), the effect of different noise products on the ENSO variability is studied. It is clearly shown that in the subcritical regime, white noise is able to excite the interannual mode (see Fig. 4a in Roulston and Neelin 2000) with qualitatively similar results as in Fig. 8.

When, instead of a variable K_H, a variable atmospheric damping of SST anomalies is considered, similar results are found. The multidecadal mode has a negative growth factor under restoring conditions for temperature, but it can be excited by atmospheric noise (Te Raa and Dijkstra 2002). Under prescribed flux conditions, the growth factor of the multidecadal mode is positive and sustained oscillations occur. The results in this subsection therefore strongly motivate to keep analyzing the supercritical regime (hence the prescribed flux case) through the modeling hierarchy because it is here that sustained oscillations occur. The latter oscillations are relatively easy to trace through a hierarchy of models, and one does not have to integrate

over a long time interval under noise forcing. Whenever such a sustained oscillation is found, it should then be kept in mind that as soon as the boundary conditions allow a stronger atmospheric damping of SST anomalies, the mode may be damped, but its spatial pattern of variability can still be excited by atmospheric noise.

A connection towards the GFDL-R30 results

The results in the previous section provide a clear hypothesis for the multidecadal variability in the GFDL-R30 results and in the observations: the AMO is caused by an internal mode of variability of the North Atlantic Ocean circulation, which is related to the existence of a Hopf bifurcation of the Atlantic's mean thermohaline circulation. The timescale of the variability is set by the basin crossing time of density anomalies in the background density field, and the propagation mechanism of SST anomalies is according to Fig. 7.

The idealized single-hemispheric configuration as in Te Raa and Dijkstra (2002) is obviously far from the GFDL-R30 model setup, and to make a strong case for our hypothesis, we would like to increase model complexity step-by-step while monitoring the mechanistic indicators. Complexities which have to be added are (1) lower lateral friction, (2) continental boundaries, (3) salinity, (4) wind forcing, (5) bottom topography, and (6) cross equatorial flow. On the other hand, there are also limits to computational resources; we are therefore limited to consider only a few intermediate steps at a time.

First results on steps 1 and 2 were presented by Te Raa et al. (2004) and indicated that the physics of the multidecadal variability in the MOM flows remains the same when lower lateral friction and realistic continental boundaries are considered. In these less idealized cases, the mechanistic

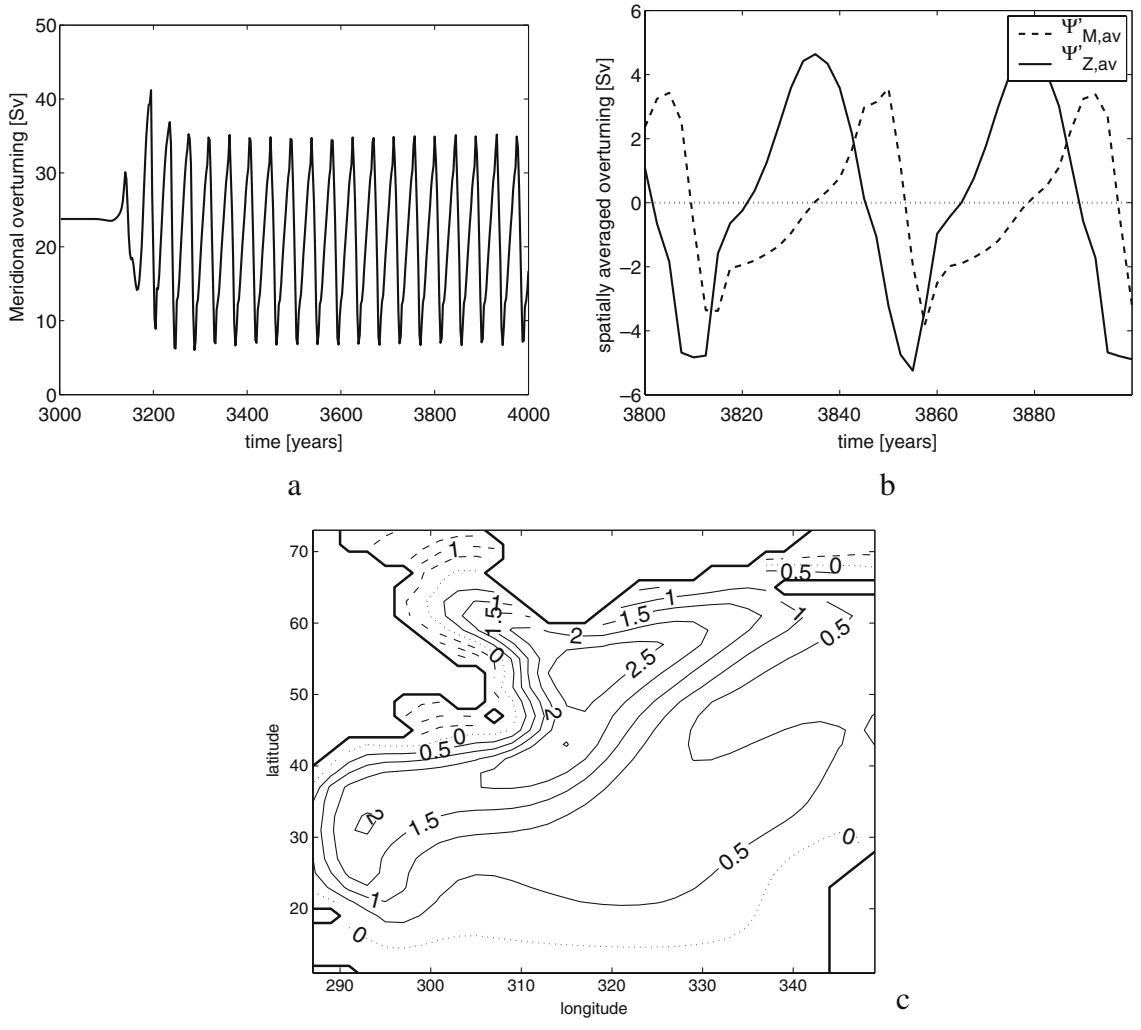

Fig. 9 **a** Maximum meridional overturning of a periodic orbit in the MOM configuration with realistic continental boundaries and a resolution of 2°×2° and 16 layers; K_H=700 m^2 s^{-1} and A_H=1.6×10^5 m^2 s^{-1}. At t=3,000 years, the boundary condition was changed to a prescribed heat flux. **b** Spatially averaged zonal (*solid*) and meridional (*dashed*) overturning anomalies. **c** Difference in SSTs between maximum and minimum meridional overturning for the oscillation in **a**

indicator M1 was found to be rather sensitive to the way the temperature differences are computed. This sensitivity to details of the computation is undesirable, and it disqualifies M1 as a useful indicator for more complex flows. However, M2 turned out to be a fairly robust indicator of the propagation mechanism over the hierarchy of models. Below, we will first present additional results for the low-friction, continental geometry configuration as in Te Raa et al. (2004) and then extend these to include salinity (step 3). The anticipated effects of the complexities (steps 4–6) not considered here will be discussed in the last section.

To connect the finite amplitude results in Te Raa et al. (2004) to the analysis of the GFDL-R30 climate model, we present here additional computations of variability in the MOM model. The resolution used is 2°×2° horizontally and 16 layers vertically; values of A_H=1.6×10^5 m^2 s^{-1} and K_H=700 m^2 s^{-1} are used for the mixing coefficients. After the spin-up under restoring conditions, the heat flux is diagnosed and then used as a prescribed flux condition. An oscillation with a period of about 45 years develops in the flow, as can be seen from a plot of the maximum of the meridional overturning streamfunction (Fig. 9a). A plot of

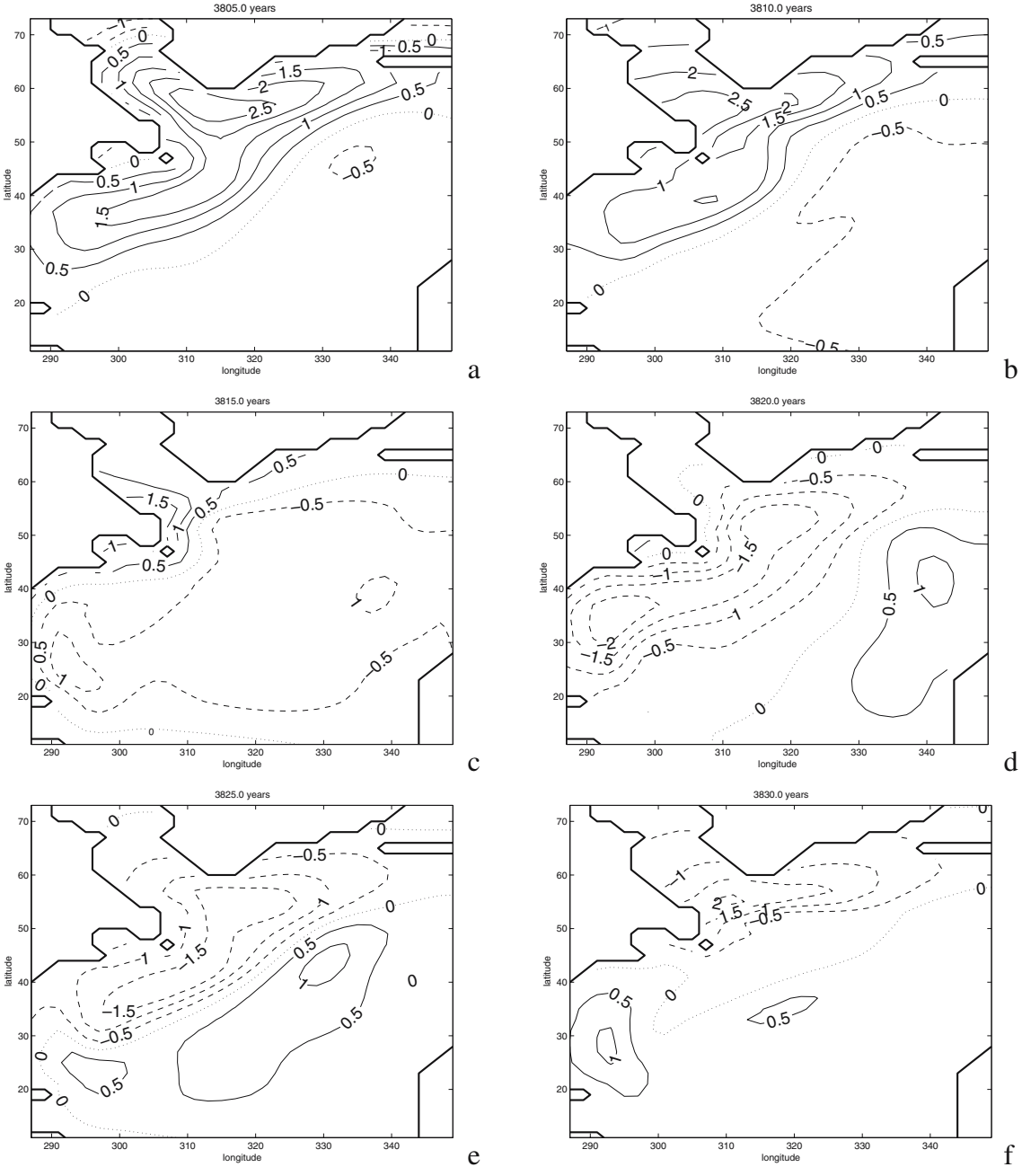

Fig. 10 Snapshots of the surface temperature anomaly (in degrees Celsius) with respect to an average over the last four oscillation periods at six times during half an oscillation cycle for the simulation in Fig. 9, at **a** t=3,805 years; **b** t=3,810 years; **c** t=3,815 years; **d** t=3,820 years; **e** t=3,825 years; and **f** t=3,830 years

the zonal and meridional overturning anomalies (Fig. 9b) shows a signature of M2. Although this is a finite amplitude flow in which the cooling phase (decreasing Ψ_M) is shorter than the warming phase (increasing Ψ_M), the phase difference M2 on the multidecadal timescale is still similar to that found in the simple configuration of Te Raa and Dijkstra (2002), with the meridional overturning anomaly lagging the zonal overturning anomaly by a quarter to one third of an oscillation period.

To compare with the GFDL-R30 results, the SST difference field between Atlantic warm (corresponding to maximum meridional overturning) and Atlantic cold (corresponding to minimum meridional overturning) states is plotted in Fig. 9c. The secondary maximum in the warm anomaly near 70°W, 30°N, the area of negative anomalies near the North American coast, and the pattern of the positive anomalies are qualitatively similar to the patterns in Fig. 5.

The patterns of the temperature anomalies for several phases in the oscillation are plotted in Fig. 10. The anomaly pattern at the maximum of the meridional overturning (Fig. 10a) has a maximum of about 2.5°C south of Greenland, and the positive anomaly slants southwestward. The negative anomalies in the eastern part of the basin are relatively weak and have a very broad scale. As time progresses and the meridional overturning decreases, the broad negative temperature anomaly propagates westward (Fig. 10b); after about one fourth of a period, the anomaly over the basin has approximately a single sign (Fig. 10c), but 5 years later (Fig. 10c), the pattern becomes more localized as it nears the continents (Fig. 10d). The pattern after 20 years is about similar to the pattern in Fig. 10a but with the signs reversed (Fig. 10e, f). Using the mechanistic indicator M2, we have demonstrated therefore that although the patterns of the multidecadal variability (Fig. 10) are strongly deformed by the continents, the mechanism of propagation is still the same as that described with the help of the multidecadal mode (as sketched in Fig. 7).

The amplitude of the oscillation in Fig. 9a is quite large and depends on the value of K_H (and also on the atmospheric damping). To show the dependence on K_H, we computed transient flows for four additional values of K_H. The sensitivity of the period and peak-to-peak amplitude of the maximum meridional streamfunction anomaly of the oscillation vs K_H is shown in Fig. 11. With increasing K_H, the period of the oscillation increases, and its amplitude decreases, just as predicted from the growth factor of the multidecadal mode (Te Raa and Dijkstra 2002). For this more complex MOM configuration, we can always tune the period and amplitude of the oscillation with the value of K_H. Within reasonable values of K_H, however, the period will always be in the 40- to 100-year, i.e. multidecadal, range.

To study the effect of salinity, we use the same configuration as above, with K_H=1,000 m^2 s^{-1}, but now

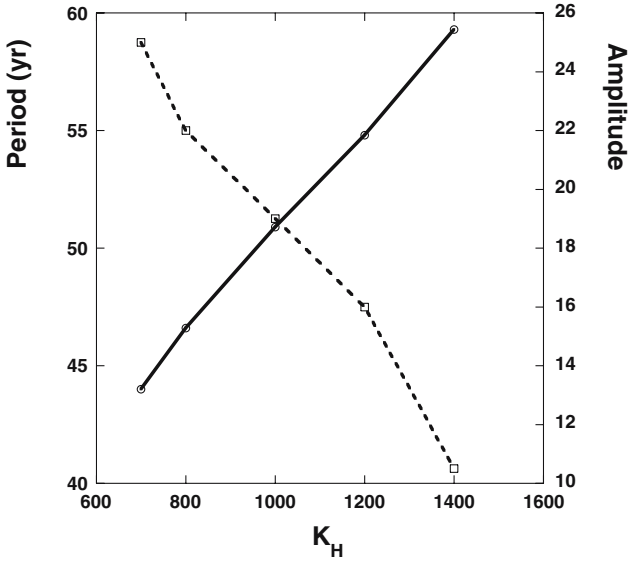

Fig. 11 Dependence of period (in years, *solid*) and amplitude of the maximum meridional overturning streamfunction (in sverdrup, *dashed*) of the multidecadal finite amplitude oscillation on K_H for the MOM configuration as in Fig. 9

during the restoring simulation, the salinity is also restored to the profile:

$$S_S(\theta) = S_0 + \frac{\Delta S}{2} \cos \pi \frac{\theta - \theta_s}{\theta_n - \theta_s}, \tag{3}$$

with S_0=35 practical salinity units (psu) and ΔS=0.5 psu; a linear equation of state and a restoring timescale of 30 days are used. The resulting equilibrium meridional overturning has a magnitude of 18 Sv. This is slightly smaller than in the temperature-only case because of the smaller pole-to-equator density gradient.

From this equilibrium flow, both the heat flux and the freshwater flux are diagnosed and prescribed over the next 2,000 years of simulation. The amplitude of the meridional overturning streamfunction displays an oscillation with a period of 91 years (Fig. 12a) and a peak-to-peak amplitude of 7 Sv. At the location 56°W, 40°N, the amplitudes of the surface temperature and salinity are shown in Fig. 12b. They are in phase, which is similar to the results in the GFDL-R30 model. The amplitudes of the temperature at two locations (56°W, 40°N and 40°W, 56°N) are plotted in Fig. 12c. There is a slight phase difference (much smaller than in the GFDL-R30 results) between the temperature signal at the two locations, with the northern location leading the southern one. The patterns of variability are very similar for both salinity and temperature and have the same spatial structures as in Fig. 10. Adding salinity as an additional complexity to these flows therefore does not change the existence and physics of the multidecadal variability.

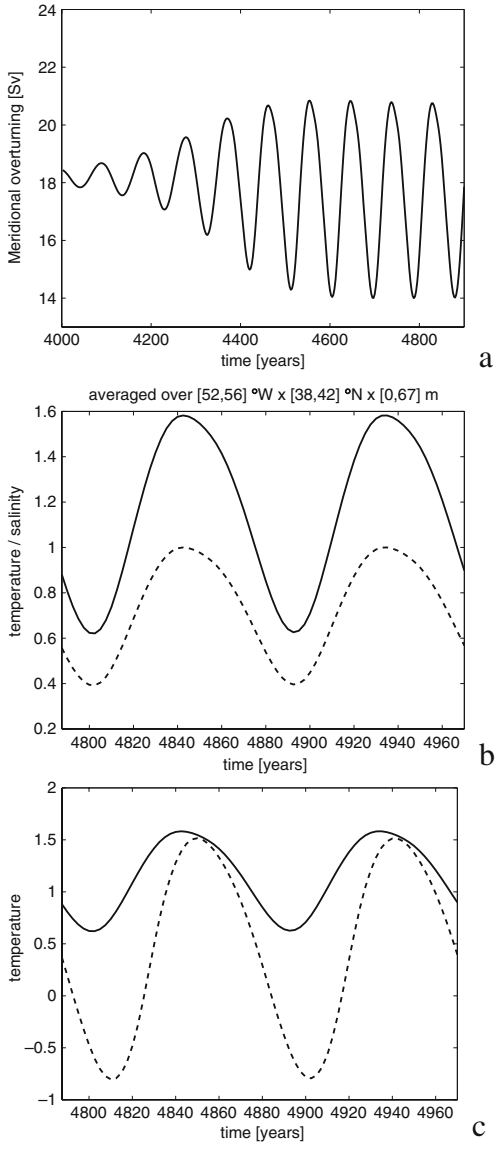

Fig. 12 **a** Maximum meridional overturning for the MOM configuration with low lateral friction, continental geometry, and salinity under prescribed flux conditions. **b** Amplitude of the scaled temperature (*T*-15) (*solid*) and normalized salinity (*S*-35)/[max (*S*-35)] (*dashed*) at the location 56°W, 40°N. **c** Scaled amplitude of the temperature anomaly at 40°W, 56°N (*T*-15, *solid*) and at 56°W, 40°N (*T*-10, *dashed*)

Summary and discussion

Analysis of the GFDL-R30 climate model results demonstrates the existence of a dominant statistical oscillatory pattern of variability with a timescale of 44 years. The SST difference pattern between high and low meridional overturning shows a good qualitative agreement with available observations (Fig. 5). The timescale and patterns of variability are also in good agreement with the earlier GFDL-R15 results (Delworth et al. 1993). It is not easy to understand the physics of this variability directly from the analysis of these GCM results.

In idealized ocean models, on the other hand, multidecadal variability appears through the destabilization of the mean three-dimensional thermohaline flow. The growth factor of this mode depends on model parameters (atmospheric damping, K_H, etc.), and it is largest under zero atmospheric damping (prescribed flux conditions) and small K_H. We have argued in Sect. 3.1 that, even if the growth factor of this mode is negative, the spatial pattern of the multidecadal mode can be excited by atmospheric noise and hence can be detected by M-SSA as a statistical mode of variability.

This raises the question of whether the physics of the multidecadal variability as found in the GFDL-R30 model is the same as that causing the multidecadal mode in the idealized models. In the latter, the timescale of the variability is set by the basin crossing time of density anomalies in a background density field and the propagation mechanism of SST anomalies is according to Fig. 7. It is also clear that this question is not so easy to answer directly since much more physical processes are represented in the GFDL-R30 model than in the idealized ocean-only models.

We have proceeded from the idealized models to add complexity in the form of more realistic continents, low lateral friction, and salinity using the MOM. Key element to determine whether the physics of the oscillation is still that of the multidecadal mode is the mechanistic indicator M2, the phase difference between meridional and zonal overturning anomalies. The indicator M2 cannot be directly applied to the GFDL-R30 results because of the presence of cross-equatorial flow. A sequence of MOM simulations shows that in a realistically shaped basin, multidecadal variability can be attributed (using M2) to the presence of the multidecadal mode. In these simulations, the salinity is not crucial to the mechanism of variability. Under prescribed flux conditions for both temperature and salinity and a linear equation of state, there is effectively only one tracer, i.e., density. With a nonlinear equation of state, such as that used in the GFDL-R30 model, deviations can in principle occur, but they are likely to be small.

For the multidecadal variability in the MOM (of which we understand the physics), the SST difference pattern between high and low meridional overturning (Fig. 9c) also shows a reasonable qualitative correspondence with that in the GFDL-R30 model and in observations. There are, however, also several discrepancies, in particular in the propagation direction of the SST anomalies. In the MOM results, this is strictly westward, while in the GFDL-R30 results, propagation is more in a southwestward direction below the surface and more stationary near the surface. This is also seen in the phase differences between the temperature anomalies in Fig. 12a (GFDL-R30) and Fig. 12c (MOM); the latter differences are much smaller.

There is an issue which troubles in the comparison of the results from the GFDL-R30 model and the MOM. The patterns of the RC 1–2 in the GFDL-R30 model are those of a dominant statistical mode of variability. In techniques such as M-SSA, additional variability, e.g., due to convection or sea-ice processes, may give a contribution

to the statistical mode on the multidecadal timescale, as can variations in atmospheric forcing. Even if the main physics is controlled by processes as sketched in Fig. 7, the statistical techniques, which are all in some way variance maximizing, pick up these additional signals, and hence, the resulting pattern on this timescale may show signatures not related to the main cause of the variability.

With respect to the surface propagation, both Huck et al. (1999) and Kravtsov and Ghil (2004) have found more stationary patterns near the surface in idealized ocean-only models. For results in both papers, however, the temperature anomalies are still westward propagating at depth. From the physical mechanism, as described by Te Raa and Dijkstra (2002), this type of propagation for the multidecadal mode is possible when the zonal surface velocities become large enough to oppose the westward propagating tendencies. A wind stress at the surface, for example, introduces eastward propagating tendencies and can induce a more stationary pattern at the surface. The essential physics is unaltered, however, since there is still westward propagation at depth, and hence, the out-of-phase velocity response due to the thermal wind balance is still according to the mechanism as in Fig. 7.

Apart from the presence of the wind stress, bottom topography and the presence of a cross equatorial flow may also contribute to a difference in propagation. From idealized ocean-only model studies, it is known that bottom topography stabilizes the thermohaline flow (Huck et al. 2001), likely leading to a decrease in growth factor of the multidecadal mode. As the mechanism of propagation of the multidecadal mode is based on thermal wind balance, it is not expected that bottom topography has much influence on the existence of the multidecadal mode, but it may modify its propagation direction and spatial pattern. It is difficult to anticipate the impact of cross-equatorial flow on the multidecadal variability. Because the spatial pattern is localized with maximum amplitudes far from the equator, the effect may be small.

As far as we have proceeded through the hierarchy of models, the hypothesis that the timescale of variability associated with the AMO is caused by the basin crossing time and its pattern is that of a deformed multidecadal mode is very plausible. This hypothesis is consistent with many, if not all, model results on multidecadal variability. It was discussed at length in Te Raa and Dijkstra (2002) that the westward propagation of the temperature anomalies within an oscillation cycle is seen in most sustained multidecadal oscillations in ocean-only models (Greatbatch and Zhang 1995; Chen and Ghil 1995; Huck et al. 1999). The different numerical simulations as done in Delworth and Greatbatch (2000) do not falsify our hypothesis. Their CLIM simulation (the ocean model forced with only climatological atmospheric fluxes) nicely demonstrates that the flow regime is not supercritical, i.e., there is no sustained oscillation. The TOTAL (ocean forced by total fluxes of the coupled model run) and RANDOM (ocean forced by only the annual-mean atmospheric fluxes chosen at random) simulations demonstrate that coupled feedbacks and also atmospheric noise on timescales less than 1 year are not needed to generate the multidecadal variability.

The simulations HEAT_LP [only low-frequency part (>20 years) of the atmospheric fluxes] and HEAT_HP [only high-frequency part (<20 years) of the atmospheric fluxes] seem at first sight puzzling. As the multidecadal variability has a much smaller amplitude under HEAT_HP, it looks like the low-frequency component of the atmospheric variability is driving the multidecadal variability, as is also the interpretation of Delworth and Greatbatch (2000). However, as shown by Roulston and Neelin (2000), the result that high-frequency noise is not able to excite the multidecadal signal is due to the fact that the underlying ocean model is only weakly nonlinear. In this case, there is no effective pathway to channel energy from the smaller to the larger scales. Consequently, the low-frequency part of the noise forcing is essential to excite the multidecadal mode. It does not mean that the variability is "driven" by the low-frequency part of the atmospheric forcing. In reality, the ocean is highly nonlinear; there is a mechanism for channeling energy over a range of scales, and hence, high-frequency atmospheric noise is capable of exciting the multidecadal mode.

While a clear mechanistic view is now available on the multidecadal SST variability that can be induced by internal ocean processes under prescribed flux conditions, the role of the atmosphere is crucial to determine the signal of the multidecadal mode in the actual North Atlantic climate. Prescribed flux conditions are a strong idealization (net zero atmospheric damping), and in reality, the SST anomalies are substantially damped by the atmosphere. The latter is expected to decrease the growth rate of the multidecadal mode. On the other hand, the atmosphere itself has a strong variability on a multitude of spatial and temporal scales which can strongly affect the multidecadal mode (Griffies and Tziperman 1995). Atmospheric variability may also enhance the energy of multidecadal frequencies either independent of dynamical ocean processes (Hasselmann 1976) or affected just by oceanic advection (Saravanan and McWilliams 1998). The interaction of the multidecadal mode with the overlying atmosphere and its low-frequency variability is the next step in the line of studies of the dynamics of Atlantic multidecadal variability and is necessary to further connect the results of idealized models with those of GCMs.

Finally, this study has demonstrated the usefulness of dynamical systems analysis, together with a hierarchy of models, to determine physical mechanisms of climate variability in complex general circulation models. The idea to isolate this mechanism in a most elementary context and then trace its characteristics through the model hierarchy provides an approach that can also be followed with respect to other phenomena of climate variability. In fact, a similar approach has already been shown to be very successful in

determining the physical mechanism of propagation of anomalies in ENSO. The existence of an underlying mode of variability which determines the multidecadal evolution of SSTs in the North Atlantic Ocean could be an important issue in long-term climate forecasting.

Acknowledgments This work was supported by the Netherlands Organization for Scientific Research (NWO) under a PIONIER grant to H.D. and NSF grant OCE-0425484. The authors thank Mathijs Schouten for his help with the M-SSA software and Tom Delworth (GFDL) for providing the GFDL-R30 data.

References

Bjerknes J (1964) Atlantic air–sea interaction. Adv Geophys 10:1–82

Chen F, Ghil M (1995) Interdecadal variability of the thermohaline circulation and high-latitude surface fluxes. J Phys Oceanogr 22:161–167

Chen F, Ghil M (1996) Interdecadal variability in a hybrid coupled ocean–atmosphere model. J Phys Oceanogr 26:1561–1578

Colin de Verdière A, Huck T (1999) Baroclinic instability: an oceanic wavemaker for interdecadal variability. J Phys Oceanogr 29:893–910

Delworth TL, Greatbatch RG (2000) Multidecadal thermohaline circulation variability driven by atmospheric surface flux forcing. J Climate 13:1481–1495

Delworth, TL, Mann ME (2000) Observed and simulated multidecadal variability in the Northern Hemisphere. Clim Dyn 16:661–676

Delworth TL, Manabe S, Stouffer RJ (1993) Interdecadal variations of the thermohaline circulation in a coupled ocean–atmosphere model. J Climate 6:1993–2011

Delworth TL, Stouffer RJ, Dixon KW, Spelman MJ, Knutson TR, Broccoli AJ, Kushner PJ, Wetherald RT (2002) Review of simulations of climate variability and change with the GFDL R30 coupled climate model. Clim Dyn 19:555–574

Dong B, Sutton RT (2005) Mechanism of interdecadal thermohaline circulation variability in a coupled ocean–atmosphere GCM. J Climate 18:1117–1135

Enfield DB, Mestas-Nuñe AM, Trimble P (2001) The Atlantic multidecadal oscillation and its relation to rainfall and river flows in the continental US. Geophys Res Lett 28:2077–2080

Folland CK, Parker DE, Kates FE (1984) Worldwide marine temperature fluctuations. Nature 310:670–673

Gray WM, Sheaffer JD, Landsea CW (1997) Climate trends associated with multidecadal variability of Atlantic hurricane activity. In: Diaz H, Pulwarthy D (eds) Hurricanes: climate and socioeconomic impacts. Springer, Berlin Heidelberg New York, pp 15–53

Greatbatch RJ, Petersen KA (1996) Interdecadal variability and oceanic thermohaline adjustment. J Geophys Res 101:20467–20482

Greatbatch RJ, Zhang S (1995) An interdecadal oscillation in an idealized ocean basin forced by constant heat flux. J Climate 8:82–91

Griffies SM, Tziperman E (1995) A linear thermohaline oscillator driven by stochastic atmospheric forcing. J Climate 8:2440–2453

Hasselmann K (1976) Stochastic climate models. I: theory. Tellus 28:473–485

Huck T, Vallis G (2001) Linear stability analysis of the three-dimensional thermally-driven ocean circulation: application to interdecadal oscillations. Tellus 53A:526–545

Huck T, Colin de Verdière A, Weaver AJ (1999) Interdecadal variability of the thermohaline circulation in box-ocean models forced by fixed surface fluxes. J Phys Oceanogr 29:865–892

Huck T, Vallis G, Colin de Verdière, A (2001) On the robustness of interdecadal modes of the thermohaline circulation. J Climate 14:940–963

Jin F-F (1997) A theory of interdecadal climate variability of the North Pacific ocean–atmosphere system. J Climate 10:1821–1835

Kerr RA (2000) A North Atlantic climate pacemaker for the centuries. Science 288:1984–1986

Kravtsov S, Ghil M (2004) Interdecadal variability in a hybrid coupled ocean–atmosphere–sea ice model. J Phys Oceanogr 34:1756–1775

Kushnir Y (1994) Interdecadal variations in North Atlantic sea surface temperature and associated atmospheric conditions. J Phys Oceanogr 7:141–157

Latif M, Roeckner E, Botzet M, Esch M, Haak H, Hagemaann S, Jungclaus J, Legutke S, Marsland S, Mikolajewicz, Mitchell J (2004) Reconstructing, monitoring and predicting multidecadal-scale changes in the North Atlantic thermohaline circulation with sea-surface temperature. J Climate 17:1605–1614

Moron V, Vautard R, Ghil M (1998) Trends, interdecadal and interannual oscillations in global sea-surface temperature. Clim Dyn 14:545–569

Neelin JD, Battisti DS, Hirst AC, Jin F-F, Wakata Y, Yamagata T, Zebiak SE (1998) ENSO theory. J Geophys Res 103:14261–14290

Plaut G, Vautard R (1994) Spells of low-frequency oscillations and weather regimes in the northern hemisphere. J Atmos Sci 51:210–236

Preisendorfer RW (1988) Principal component analysis in meteorology and oceanography. Elsevier, Amsterdam

Roulston M, Neelin JD (2000) The response of an ENSO model to climate noise, weather noise and intraseasonal forcing. Geophys Res Lett 27:3723–3726

Saravanan R, McWilliams J (1998) Advective ocean–atmosphere interaction: an analytical stochastic model with implications for decadal variability. J Climate 11:165–188

Schlesinger ME, Ramankutty N (1994) An oscillation in the global climate system of period 65–70 years. Nature 367:723–726

Sutton RT, Hodson DLR (2005) Atlantic Ocean forcing of North American and European summer climate. Science 309:115–118

Te Raa LA, Dijkstra HA (2002) Instability of the thermohaline ocean circulation on interdecadal time scales. J Phys Oceanogr 32:138–160

Te Raa LA, Dijkstra HA (2003a) Modes of internal thermohaline variability in a single-hemispheric ocean basin. J Mar Res 61:491–516

Te Raa LA, Dijkstra HA (2003b) Sensitivity of North Atlantic multidecadal variability to freshwater flux forcing. J Climate 32:138–160

Te Raa LA, Gerrits J, Dijkstra HA (2004) Identification of the mechanism of interdecadal variability in the North Atlantic Ocean. J Phys Oceanogr 34:2792–2807

Tourre YM, Rajagopalan, Kushnir Y (1999) Dominant patterns of climate variability in the Atlantic Ocean during the last 136 years. J Climate 12:2285–2299

Venegas S, Mysak L (2000) Is there a dominant timescale of natural climate variability in the Arctic? J Climate 13:3412–3434